Biosensors and Bioelectronics 98 (2017) 357–363

Contents lists available at ScienceDirect

Biosensors and Bioelectronics

journal homepage: www.elsevier.com/locate/bios

Quantitative detection of glucose level based on radiofrequency patch biosensor combined with volume-fixed structures

Tian Qiang[a], Cong Wang[b,*], Nam-Young Kim[a,*]

[a] Department of Electronic Engineering, Kwangwoon University, Seoul, Republic of Korea
[b] Department of Microwave Engineering, Harbin Institute of Technology, Harbin, China

ARTICLE INFO

Keywords:
Radiofrequency patch
Quantitative detection
Volume-fixed structures
Glucose level detection
Excellent biosensing performance

ABSTRACT

A concept for characterizing a radiofrequency (RF) patch biosensor combined with volume-fixed structures is presented for timely monitoring of an individual's glucose levels based on frequency variation. Two types of patch biosensors—separately integrated with a backside slot (0.53 μL) and a front-side tank (0.70 μL) structure—were developed to achieve precise and efficient detection while excluding the effects of interference due to the liquidity, shape, and thickness of the tested glucose sample. A glucose test analyte at different concentrations (50–600 mg/dL) was dropped into the volume-fixed structures. It fully interacted with the RF patch electromagnetic field, effectively and sensitively changing the resonance frequency and magnitude of the reflection coefficient. Measurement results based on the resonance frequency showed high sensitivity up to 1.13 MHz and 1.97 MHz per mg/dL, and low detection limits of 26.54 mg/dL and 15.22 mg/dL, for the two types of patch biosensors, respectively, as well as a short response time of less than 1 s. Excellent reusability of the proposed biosensors was verified through three sets of measurements for each individual glucose sample. Regression analysis revealed a good linear correlation between glucose concentrations and the resonance frequency shift. Moreover, to facilitate a multi-parameter-sensitive detection of glucose, the magnitude of the reflection coefficient was also tested, and it showed a good linear correlation with the glucose concentration. Thus, the proposed approach can be adopted for distinguishing glucose solution levels, and it is a potential candidate for early-stage detection of glucose levels in diabetes patients.

1. Introduction

Aqueous glucose solutions play a fundamental role in many biomedical processes in various chemical and biological systems. Therefore, sensitive detection of glucose concentration in water may be useful for studying biomedical properties (Wang, 2001; Kim, Dhakal et al., 2015; Yilmaz et al., 2014). Diabetes mellitus, commonly referred to as diabetes, is a disease caused by a metabolic disorder characterized by fluctuations in the blood glucose level outside the normal range. Such fluctuations result from either insufficient insulin production by the beta cells in the pancreas or the body's resistance to the action of insulin. For early detection and treatment of diabetes, it is important to monitor the glucose level of an individual suspected of having the disease (Aloraefy et al., 2014; Kim et al., 2013; Ricci et al., 2005; Hu et al., 2012; Abdalla et al., 2010).

Recently, biosensor design based on radiofrequency (RF) techniques has attracted considerable attention, and wide-ranging biomedical applications have been researched, such as bimolecular binding (Lee et al., 2012), DNA sensing (Lee et al., 2010), human cell dielectric spectroscopy (Dalmay et al., 2009), and stress biomarker characterization (Lee et al., 2013). Based on the interaction between microwave electromagnetic fields and the concentrations or physical characteristics of tested samples, the RF biosensor mechanism can be investigated through changes in the equivalent inductance and capacitance, center frequency, or magnitude of S-parameters. Moreover, the RF biosensor is considered as a promising and competitive candidate for implementing third-generation glucose biosensors for mediator-free glucose detection (Adhikari and Kim, 2016) owing to its advantages of easy fabrication, quick response time, high selectivity, and tolerable linearity. Furthermore, precise and efficient detection with a fixed testing area, stable shape, and quantified and minimized volume of testing samples should also be considered to prevent interference in the measurement tolerance by the liquidity, shape, and thickness of the tested sample (Ouyang et al., 2007; Siddiqui et al., 2012; Mirasoli et al., 2013; Rosa et al., 2015). Because the biosensor RF performance is closely related to the effective dielectric constant of the glucose sample, it is severely affected by the thickness and volume of the tested sample. Therefore, quantitative detection is crucial. During each test, the

* Corresponding authors.
E-mail addresses: kevinwang@hit.edu.cn (C. Wang), nykim@kw.ac.kr (N.-Y. Kim).

http://dx.doi.org/10.1016/j.bios.2017.06.057
Received 18 March 2017; Received in revised form 26 June 2017; Accepted 27 June 2017
Available online 28 June 2017
0956-5663/

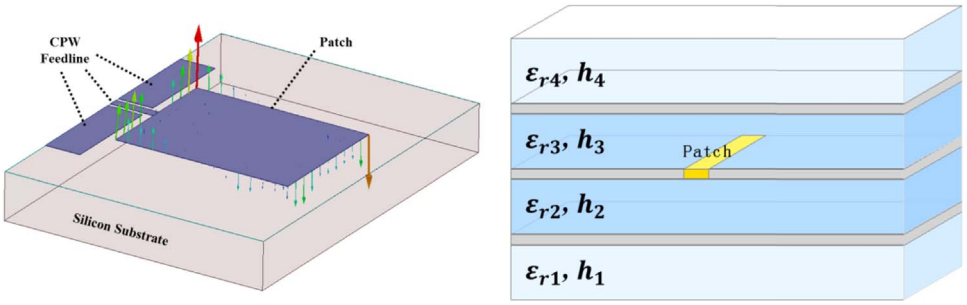

Fig. 1. (a) Electric field of the patch at resonance frequency and (b) cross-sectional view of the proposed patch biosensor with multiple layers.

sample should be stable, i.e., thickness-, volume-, and location-fixed, identical to the previous measurement condition.

In this work, we propose precise and quantitative detection of glucose levels on the basis of RF patch biosensor combined with volume-fixed structures. Two types of RF biosensors are developed: one has a backside slot structure with a volume of approximately 0.53 μL (2.5 mm × 2.0 mm × 0.106 mm), and the other has a front-side tank structure with a volume of approximately 0.70 μL (2 mm × 3.3 mm × 0.106 mm). Less than 1 μL of the testing sample is required, resulting in minimal consumption of the sample. Further, different concentrations of glucose can generate different effective dielectric constants; therefore, the electromagnetic field of the patch can be interfered by closely contacted samples. The variations in the resonance frequency and magnitude of the reflection coefficient acquired for various glucose concentrations ranging from 50 mg/dL to 600 mg/dL are efficiently characterized for glucose-level detection. Furthermore, to increase the patch biosensor sensitivity, the backside slot and front-side tank are constructed to be significantly larger than the entire patch in order to ensure that the patch will be fully covered by the tested glucose sample and the electromagnetic field will be fully engaged in the interaction accordingly. Moreover, a remarkably quick response time of less than 1 s can be realized because of the close contact as soon as the tested glucose is dropped into the volume-fixed structures. Excellent reusability of the proposed biosensor is verified through measurements conducted three times for each glucose sample. The final measurements of the patch biosensors with backside slot and front-side tank structures indicated sensitivities of 1.13 MHz and 1.97 MHz (with a variation of 1 mg/dL in the testing glucose), detection limits of 26.54 mg/dL and 15.22 mg/dL, and compact sizes with total volumes of 2.5 mm × 2.5 mm × 0.4 mm and 2.6 mm × 3.5 mm × 0.5 mm, respectively. Thus, the proposed RF methodology is applicable to advancing the field of glucose sensing.

2. Materials and methods

2.1. Patch biosensor operating mechanism

We selected a rectangular patch, which is the most widely employed configuration and is easy to analyze using transmission-line models, fed by a coplanar waveguide (CPW) for the biosensor application in the Ku band for ensuring minimal glucose sample consumption. The patch dimensions are finite along the length and width, and the electromagnetic fields at the patch edges undergo fringing. Therefore, considering the fringing effects, the resonance frequency of the proposed patch at dominant TM_{010} mode can be deduced as

$$f_{TM_{010}} = \frac{c}{2L_{eff}\sqrt{\varepsilon_{reff}}}, \tag{1}$$

$$L_{eff} = L+2\Delta L, \tag{2}$$

where c is the speed of light in free space, L_{eff} and ε_{reff} are the effective length and dielectric constant of the patch, respectively, L is the patch length, and ΔL is the extended length along the patch owing to the fringing effect. A well-known and practical approximate relation for the normalized extension of the length, ΔL, is employed; it is given by (Balanis, 2005)

$$\Delta L = 0.412h\frac{(\varepsilon_{reff}+0.3)(\frac{W}{h}+0.264)}{(\varepsilon_{reff}-0.258)(\frac{W}{h}+0.8)}, \tag{3}$$

where W is the patch width and h is the substrate height. Based on Eqs. (1)–(3), the resonance frequency at dominant TM_{010} mode can be reproduced as

$$f_{TM_{010}} = \frac{2c\varepsilon_{reff}^{-\frac{1}{2}}}{L+0.824h(\varepsilon_{reff}+0.3)(\varepsilon_{reff}-0.258h)^{-1}(W+0.264h)(W+0.8h)^{-1}}. \tag{4}$$

When the length, width, and substrate height are fixed, the resonance frequency of the proposed patch is proportional to the effective dielectric constant, ε_{reff}. Further, the proposed patches are designed on the basis of Eqs. (1)–(4), and they operate at Ku band with a CPW feedline. The High Frequency Structure Simulator (HFSS) was employed to simulate the CPW-fed patch with volume-fixed structures. Finally, a miniaturized chip size as well as minimal volume of the volume-fixed structures can be achieved.

2.2. Patch biosensor permittivity analysis

As shown in Fig. 1(a), the electric field of the CPW-fed patch is demonstrated at the resonance frequency. It can be observed that the electric field appears perpendicular to the patch surface, and such an electric field could be affected by another dielectric material closely placed above or below the patch surface, resulting in a different ε_{reff} value. In this work, glucose samples are applied as the dielectric material. The proposed patch biosensor can be regarded as a multilayer structure considering of air, a microstrip pattern, a silicon substrate, and a glucose layer. For quasi-static analysis of multilayer microstrip transmission lines having two or more dielectric interfaces, the variation method is found to be the simplest (Bahl, 2003). Fig. 1(b) shows cross-sectional views of the proposed patch biosensor with multiple layers.

For the patch biosensor with a backside slot structure—corresponding to a two-layer open-microstrip mechanism—$h_3 = 0$ and $h_4 = \infty$, where ε_{r1}, h_1 and ε_{r2}, h_2 represent the dielectric constant and thickness of the glucose layer and silicon substrate, respectively. The effective dielectric constant can be derived as

$$\varepsilon_{patch\ biosensor\ with\ backside\ slot} = \frac{C}{C_a}, \tag{5}$$

$$\frac{1}{C} = \frac{1}{\pi\varepsilon_0 Q^2}\int_0^{\infty} \frac{f^2(\beta)d(\beta h)}{\left[\varepsilon_{r1}\frac{\varepsilon_{r2}+\varepsilon_{r1}\tanh(\beta h_2)\tanh(\beta h_1)}{\varepsilon_{r1}\tanh(\beta h_2)+\varepsilon_{r2}\tanh(\beta h_1)}+1\right](\beta h)}. \quad (6)$$

For the patch sensor with a front-side tank structure—corresponding to a shielded microstrip mechanism—$h_2 = h_3 = 0$, where ε_{r1}, h_1 and ε_{r4}, h_4 are the dielectric constant and thickness of the silicon substrate and glucose layer, respectively. The effective dielectric constant can be derived as

$$\varepsilon_{patch\ biosensor\ with\ front-side\ tank} = \frac{C}{C_a}, \quad (7)$$

$$\frac{1}{C} = \frac{1}{\pi\varepsilon_0 Q^2}\int_0^{\infty} \frac{f^2(\beta)d(\beta h)}{[\varepsilon_{r1}\coth(\beta h_1)+\varepsilon_{r4}\coth(\beta h_4)](\beta h)}, \quad (8)$$

where Q denotes the total charge on the strip conductor, β is the Fourier transform variable, and ε_0 is the free-space permittivity. The capacitance per unit length of the microstrip for the two above-mentioned types of dielectric layers is denoted as C. The capacitance C_a is determined when all the dielectric layers are replaced by air. For the two proposed patch biosensors, the value of Q, the silicon dielectric constant, and the silicon substrate thickness are fixed. It can be inferred that the effective dielectric constant is mainly determined by the thickness and dielectric constant of the glucose layer. Therefore, the variation of the dielectric constant with different glucose concentrations results in discrepancies of ε_{reff} in the patch (Dhakal et al., 2015) and affects the resonance frequency of the patch biosensor.

2.3. Device concept and fabrication

The flowchart and fabrication schematic of the patch biosensor are shown in Fig. 2(a) and (b), respectively. A 6-in. silicon wafer (thickness, 400 μm) is adopted as the substrate on account of its high etching selectivity. Step 1: A 200-nm-thick SiO_2 passivation layer is deposited by low-pressure chemical vapor deposition (LPCVD) after the wafer cleaning process, yielding a flat surface that overcomes the defects and roughness problem of the bare silicon wafer. Step 2: Ti/Au with a thickness of 20/80 nm is sputtered as the seed metal to improve metal adhesion between the substrate and the subsequently electroplated Cu/Au metal. Step 3: A photo-resistor (PR) is employed to define the Cu/Au metal structure. Step 4: Cu/Au metal with a thickness of 4.5/0.5 μm is electroplated to form the patch biosensor pattern. Here, a thicker copper layer is applied because of its relatively excellent conductivity, easy solderability, high-speed operation, and low cost compared to a pure gold layer. Step 5: The defined PR is stripped off using acetone solution in the lift-off machine. Step 6: A reactive ion etching (RIE) process using an inductively coupled plasma etcher with Ar as the etching gas is adopted to remove the undesired seed metal to prevent shorting. At this point, the basic patch structure, denoted as the sample patch, is finished and set aside for the backside-slot and front-side-tank fabrication processes.

To form the backside slot structure, Bosch deep RIE is applied to the sample patch. The AMS 200 silicon deep etcher device is employed for the Bosch etching process with 250 sccm of SF_6 under the following conditions: pressure of 4.5×10^{-2} mbar, coil power of 2700 W, bias power of 35 W, and chuck temperature of − 10 °C. The Bosch passivation process uses 80 sccm of C_4F_4 under the following conditions: pressure of 2.8×10^{-2} mbar and coil power of 1800 W. Under these conditions, 64 cycles of the Bosch process are conducted with an etching rate of 10 μm/min for 11 min and a high selectivity of more than 50: 1 (silicon: PR). Finally, a hydrophilic treatment is applied, in which the sample wafer is exposed to Ar for around 30 s using RIE with a chamber pressure of 100 mTorr, gas flow rate of 30 sccm, RF power of 150 W, and substrate electrode bias voltage of 125–280 V, followed by a cleaning process in an RCA-1 solution (NH_3: H_2O_2: H_2O, 70 °C) and DI water (Suni et al., 2002), to ensure that the tested sample can smoothly and evenly cover the slot surface. To realize front-side tank structure based on the sample patch, SU-8 2100 is chosen as the structural photoresist. First, the hydrophilic treatment described above is performed, followed by an N_2H_2/O_2 plasma surface treatment before coating of negative SU-8 2100 PR. Under a temperature of 100 °C and spin speed of 300 rpm for 120 s with an acceleration of 10 rpm/s, excellent density and roughness can be achieved for the coated SU-8 2100. Subsequently, soft baking (65 °C, 5 min), UV radiation exposure (240 mJ/cm^2), post-exposure baking (95 °C, 5 min), development (SU-8 developer, 30 min), DI water cleaning, and hard baking (150 °C, 20 min) are conducted.

Fig. 3(a) and (b) show the structures of the fabricated patch biosensors with a backside slot and a front-side tank, respectively. Microscope images clearly illustrate the main biosensor parts, as shown in Fig. 3(a-i), (a-ii), and (a-iii) for the backside slot, and Fig. 3(b-i) and (b-ii) for the front-side tank. A surface profiler is employed to

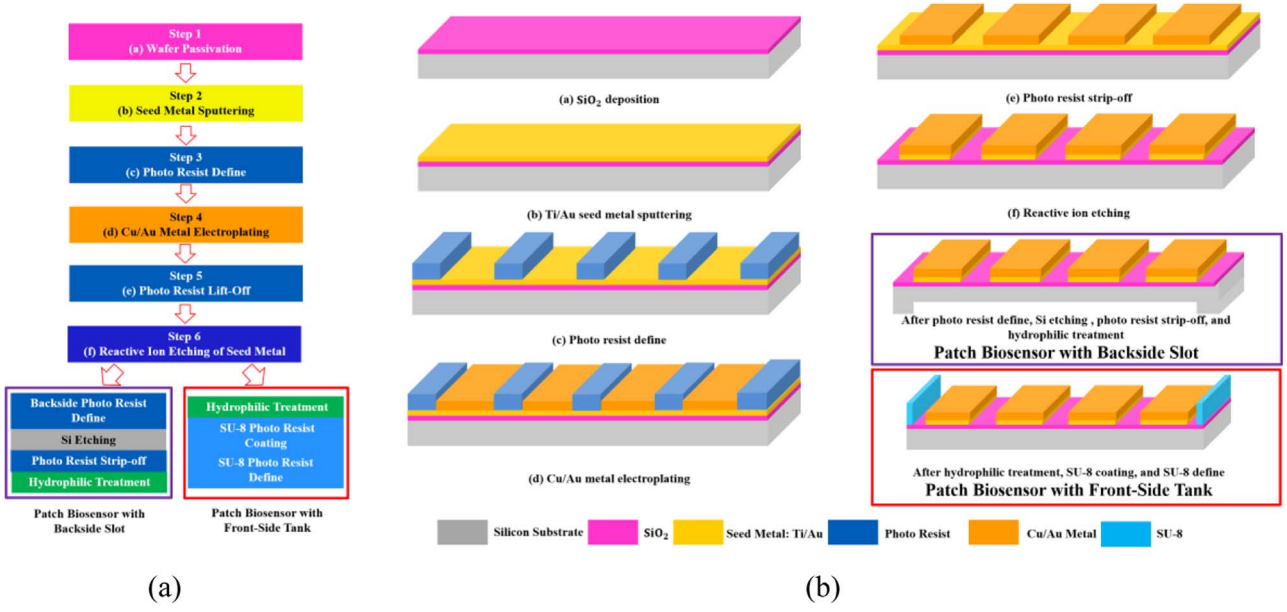

Fig. 2. (a) Flowchart and (b) cross-sectional view of the detailed fabrication schematic of the patch biosensors.

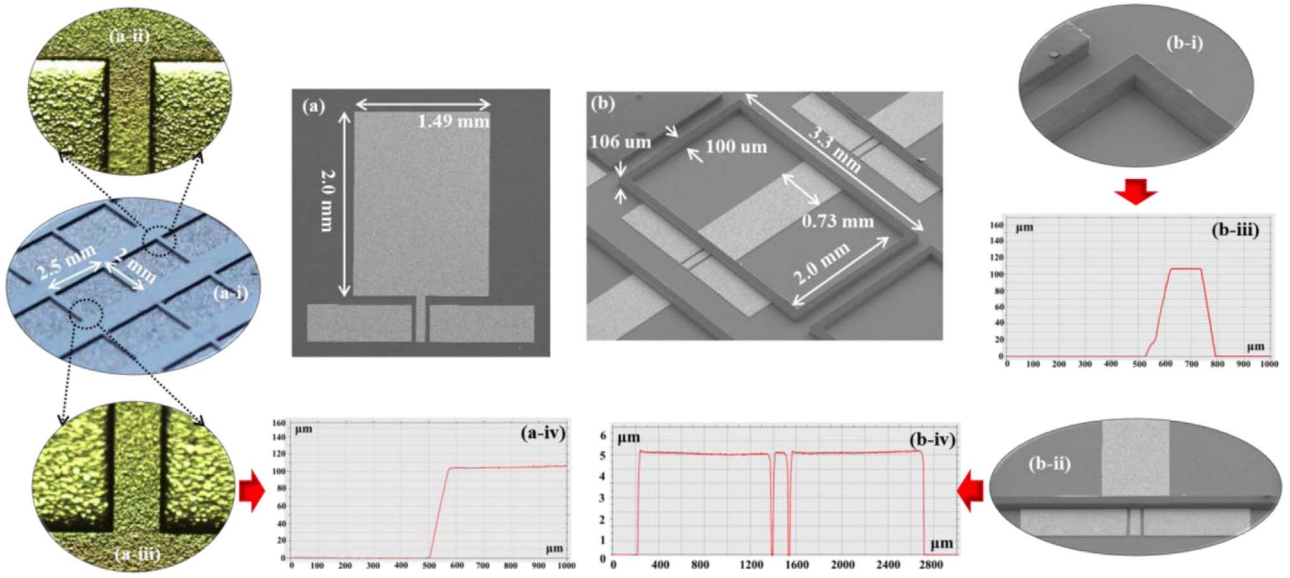

Fig. 3. Structures of the fabricated patch biosensors with a backside slot and a front-side tank: (a) patch biosensor image with backside slot, (a-i) backside slot, (a-ii) slot upper-right part, (a-iii) slot lower-left part, (a-iv) depth measurement of slot lower-left part; (b) patch biosensor image with front-side tank, (b-i) tank upper-left part, (b-ii) lower part of patch, (b-iii) tank thickness measurement, and (b-iv) patch metal thickness measurement.

accurately detect the depth and thickness at the wafer surface on the above-mentioned main parts. The backside slot with a length and width of 2.5 mm × 2.0 mm, and a depth of approximately 106 µm, is obtained, as shown in Fig. 3(a-i) and (a-iv), respectively. The front-side tank with a length and width of 3.3 mm × 2.0 mm, and a height of approximately 106 µm, is obtained along with 5-µm-thick Cu/Au metal, as shown in Fig. 3(b), (b-iii), and (b-iv), respectively. The slight fluctuation of the horizontal line in Fig. 3(a-iv) and (b-iv) is due to the rough surface of the backside slot and front-side metal owing to the hydrophilic treatment.

3. Results and discussion

The development trends of biosensing devices are toward smaller size, non-invasiveness, and integration with quantitative structures for sample handling. The motivation of this work is to achieve quantitative detection and small-volume consumption of a glucose sample while maintaining excellent properties of the biosensor, including high selectivity, quick response time, and reusability. A patch is an attractive candidate for biosensor applications because of its low profile, light weight, low manufacturing cost, and sensitive response when a glucose sample contacts the patch surface (Zhang et al., 2017; Boukarkar et al., 2017). After the patch is fabricated with volume-fixed structures, the target performance can be achieved and verified through measurements as described below.

3.1. Sample presentation and RF detection methods

Samples of D-glucose aqueous solution consisting of a mixture of DI water (Merck Millipore, Billerica, MA, USA) and D-glucose powder (Sigma-Aldrich, St. Louis, MO, USA) were prepared at nine concentrations: 25, 50, 100, 200, 300, 400, 500, 600, and 1000 mg/dL. RF detection of the glucose concentration is based on the resonance concept of the patch biosensor, which produces a reasonable shift in the resonance frequency as well as a variation in the signal amplitude. Therefore, to perform the patch-biosensor RF response measurement, a probe station was used, as shown in Fig. 4. The glucose samples were directly placed in the respective backside slot and front-side tank using a mLINE pipette (0.1–3 µL, Sartorius, Gottingen, Germany). The pipette was set at 0.53 µL and 0.70 µL, separately, and flat surfaces could be observed after the glucose sample was dropped into the slot and tank; thus, the volume specification of our proposed volume-fixed concept could be verified. For the following tests, regular pipettes, such as medical syringes, could be used instead of the expensive mLINE pipette. The frequency responses were measured over a frequency range of 10–25 GHz. To maintain the samples at a constant temperature and humidity, they were all equilibrated to room temperature and humidity prior to testing. To measure the effectiveness of this equilibration, the temperature of each sample was measured with a thermocouple probe immediately prior to RF measurement (Tura et al., 2010). The measured temperatures and relative humidities of the individual samples ranged from 22.1 °C to 22.6 °C and 14.1–14.3%, respectively. After RF measurement of a sample, the backside slot and front-side tank were flushed several times first with phosphate-buffered saline (1x PBS, pH = 7.4, consisting of 137 mmol/L NaCl, 2.7 mmol/L KCl, 10 mmol/L Na_2HPO_4, and 2 mmol/L KH_2PO_4, prepared by the Department of Biochemistry and Molecular Biology, Medical College, KyungHee University, Seoul, S. Korea) and then with DI water to remove the glucose sample prior to measuring the next sample. Finally, the DI water was cleaned with KIMTECH science wipers and the biosensor was ready for the next measurement.

3.2. RF Responses of the devices

The measured reflection coefficients of the bare patch and the patch dropped with DI water and PBS solution are shown in Fig. 5(a) and (b) for the patch biosensor with a backside slot and a front-side tank, respectively. Bare-chip resonance frequencies of 21.09 GHz and 17.25 GHz were obtained for the patch biosensor with a backside slot and a front-side tank, respectively, and the resonance frequency showed a downward shift after PBS and DI water were separately dropped into the volume-fixed structures. Because the viscosity of DI water is lower than that of the glucose sample and PBS solution, it has the highest value of ε_{reff} and produces the maximum downward shift of the center frequency after it is dropped into the volume-fixed structures (Yoon, 2011). Then, we performed an experiment with different concentrations of glucose ranging from 25 mg/dL up to 1000 mg/dL. When the bare patch was filled with glucose at increasing concentrations, the resonance peak shifted upward with a regular change in amplitude on account of the variation in the effective dielectric constant. The resonance frequency of the patch filled with glucose solution for the backside slot and front-side tank structures varied in

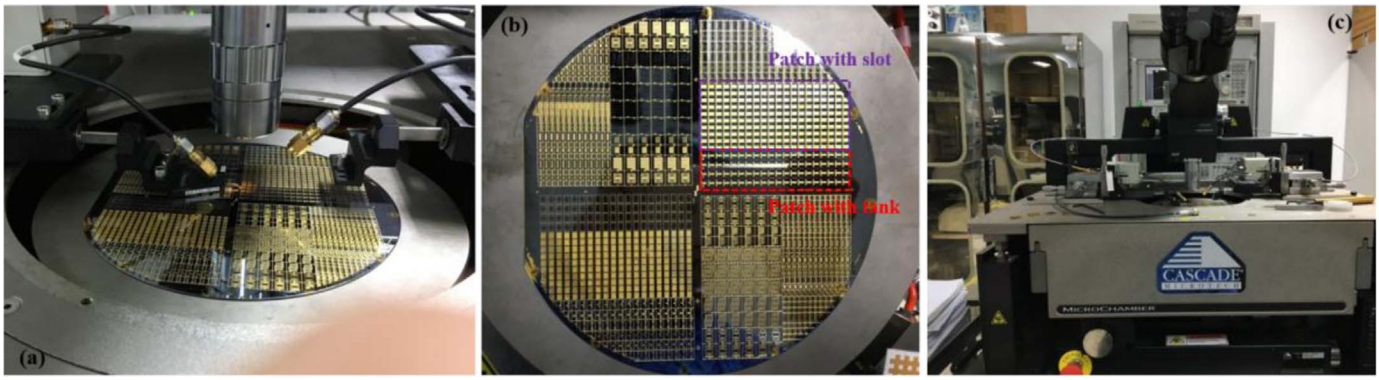

Fig. 4. Setup for S-parameter measurement of the patch biosensor: (a) patch biosensor under testing, (b) fabricated bare wafer, and (c) probe station.

the range of 18.84–19.82 and 13.09–15.23 GHz, respectively, with a tolerable shift in the resonance frequency, as shown in Fig. 5(c) and (d). A maximum shift of 2.25 GHz and 4.16 GHz, respectively, was generated at the lowest glucose level of 25 mg/dL compared with the bare patch.

Regression analysis revealed a good linear correlation between the glucose concentration and the shift in the center frequency, as shown in Fig. 6(a) and (b), and a magnitude shift of S_{11}, as shown in Fig. 6(c) and (d). The related linear regression equations are stated below.

Patch biosensor with backside slot:

y_1[GHz] = 0.00113 × x[mg/dL] + 18.91961,

linear correlation R^2 = 0.90470,

for resonance frequency, glucose concentration of 25–1000 mg/dL;

y_2[dB] = 0.00178 × x[mg/dL]–13.1927, linear correlation R^2 = 0.98712,

for magnitude of S_{11}, glucose concentration of 50–600 mg/dL;

Patch biosensor with front-side tank:

y_1[GHz] = 0.00197 × x[mg/dL] + 13.33439,

linear correlation R^2 = 0.96823,

for resonance frequency, glucose concentration of 25–1000 mg/dL;

y_2[dB] = − 0.00207 × x[mg/dL]–12.30615, linear correlation R^2 = 0.97848,

for magnitude of S_{11}, glucose concentration of 50–600 mg/dL;

where y_1 and y_2 represent the resonance frequency and magnitude of S_{11}, respectively, and x represents the glucose solution concentration. The analysis indicates that the resonance identification approach can be applied to glucose level detection. Moreover, the S_{11} value also shows a good linear correlation with the glucose level in the range of 50–600 mg/dL, which facilitates multi-parameter-sensitive detection of glucose with the proposed biosensors. A proportional difference in the fitted line exists between Fig. 6(c) and (d), where a direct proportion and an inverse proportion are observed for the patch biosensor with the backside slot and front-side tank structures, respectively. Such a phenomenon is mainly attributed to the impedance matching between the feeding network (CPW structure) and the patch

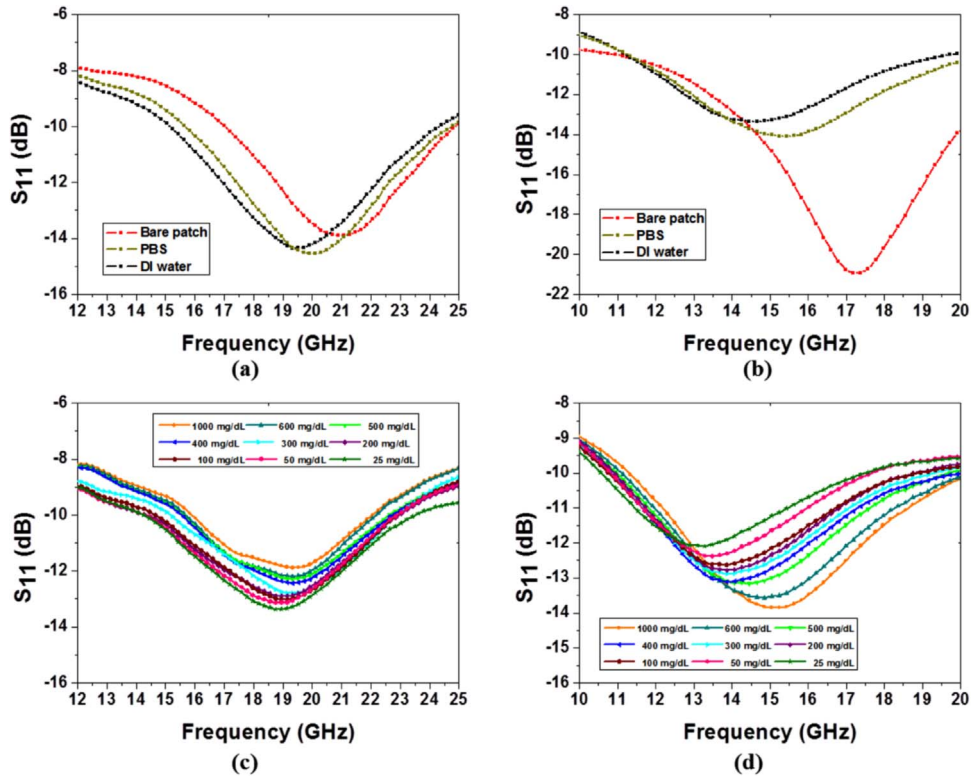

Fig. 5. Shift in resonance frequency under various conditions: (a) backside slot structure and (b) front-side tank structure. Shift in center frequency and reflection coefficient (S_{11}) magnitude for glucose samples of varying concentrations (25–1000 mg/dL): (c) backside slot structure and (d) front-side tank structure.

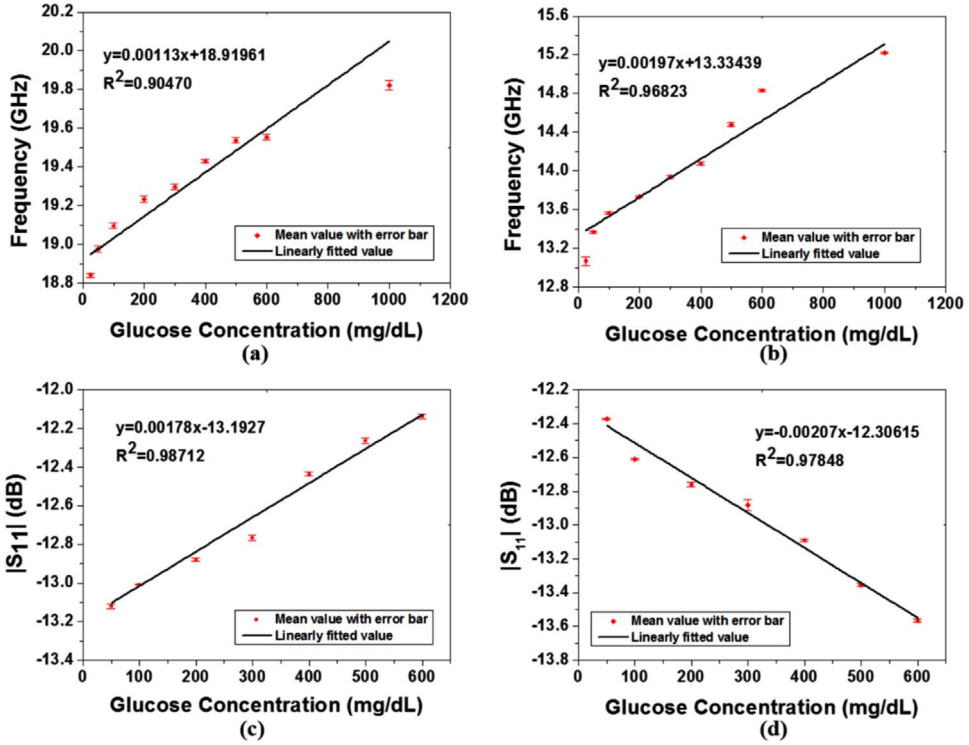

Fig. 6. Linearly fitted resonance frequency, including the mean value of resonance frequencies with error bars: (a) backside slot structure (R^2 = 0.90470, RSD < 1%) and (b) front-side tank structure (R^2 = 0.96823, RSD < 1%). Linearly fitted magnitude of S_{11}, including the mean value of S_{11} magnitudes with error bars: (c) backside slot structure (R^2 = 0.98712, RSD < 1%) and (d) front-side tank structure (R^2 = 0.97848, RSD < 1%).

during the variation of the effective dielectric constant. The impedance of the feeding network in this work is fixed at 50 Ω; therefore, if the characteristic impedance of the patch is closer to 50 Ω, the impedance matching between the feeding network and the patch will be better, resulting in a greater increase in the magnitude of the reflection coefficient (Balanis, 2005). For the two proposed biosensor types, as long as the glucose concentration ranges from 50 mg/dL to 600 mg/dL, the characteristic impedance of the patch with a backside slot structure deviates from 50 Ω, while the characteristic impedance of the patch with a front-side tank structure approaches 50 Ω. Therefore, for the patch biosensor with a backside slot structure, the magnitude of reflection coefficient decreases from − 13.12 dB to − 12.13 dB as the glucose concentration increases; for the patch biosensor with a front-side tank structure, the magnitude of reflection coefficient increases from − 12.37 dB to − 13.56 dB as the glucose concentration increases.

Table S1, S2 and Tables S3, S4 in the Supplementary section respectively summarize the resonance frequency variation and S_{11} magnitude variation under different concentrations of glucose solution for the patch biosensor with a backside slot and a front-side tank. The sensing limitation of the proposed devices, known as the limit of detection (LOD), was calculated on the basis of following equation (ICH Harmonized Tripartite Guideline, 1996) as 26.54 mg/dL and 15.22 mg/dL, respectively.

$$\mathrm{LOD} = 3.3 \times SD/m,$$

where *SD* is the standard deviation of the frequency response and *m* is the slope of the regression line. The nature of the calibration curves and the data obtained from the frequency shifted with a relative standard deviation (RSD) of less than 1% for the patch biosensor, indicating a small spread of the resonance frequencies for a particular concentration. A comparative analysis based on the performance is summarized in Table S5, where the response time is superior to that achieved in other studies and the sensitivity is fairly good compared to the resonator-based results. Fabricated volume-fixed structures facilitate quantitative detection of the glucose sample, excluding the effects of interference due to the liquidity, shape, and thickness of the tested glucose sample, thereby yielding accurate measurements. Furthermore, only a small volume (no more than 1 μL) of the glucose sample is required for the detection, resulting in minimal consumption of the sample. In addition, commonly used and cost-effective pipettes, such as medical syringes, can be allowed for testing in this work instead of expensive and strict quantitative pipettes. Thus, this approach can be regarded a potential candidate for early-stage detection of glucose levels in diabetes patients.

3.3. Reusability and real-time identification ability

The biosensor reusability was characterized by measuring the resonance frequency before and after using the glucose solution. Three different sets of experiments for each glucose concentration were performed to observe the resonance frequency for each iteration of the experiment. A total of 54 different experiments for all the glucose samples were conducted and are represented by the scatter shown in Fig. S1 (Supplementary section). There was no device response deterioration over these iterations of the measurement process. The observed data showed no overlapping of the resonance frequency among the concentrations for different sets of the experiment. Thus, it was verified that the proposed device could be reused many times after the initial use by rinsing it with PBS and DI water. The bare resonance frequencies of the two biosensor types from each set of experiments after rinsing were obtained at 21.09 GHz and 17.25 GHz, respectively, which confirmed the stability and reusability of the proposed biosensor system.

The device sensitivity was reflected by the time required for the final output. To analyze the effectiveness of the proposed biosensor, we measured the response time after the glucose solution was dropped into the front-side tank. The frequency response could be obtained on the screen of the probe station within no more than 1 s, which demonstrated satisfactory real-time identification of the glucose level by the proposed biosensor. The real-time property of the biosensor

with a backside slot was not tested owing to the difficulty in the measuring process required to place the glucose sample in the backside slot during the RF response measurement on the probe station.

4. Conclusion

This paper proposed a mediator-free and reusable RF-based glucose biosensor consisting of a rectangular patch fed by a CPW structure. By employing volume-fixed structures, namely a backside slot (0.53 μL) and a front-side tank (0.70 μL), glucose level detection could be achieved precisely and with minimum consumption of glucose over a wide range of 50–600 mg/dL. In addition, excellent biosensing performance was achieved. Even though a non-invasive technique was not realized in this work, the proposed biosensor can still be regarded as a potential and competitive candidate for early-stage detection of glucose levels in diabetes patients. Future studies should concentrate on RF performance tests based on human serum samples as well as on the design of other RF devices with non-invasive testing techniques.

Declaration of Interest

The authors declare no conflict of interest.

Acknowledgements

This work was supported by the Commercializations Promotion Agency for R & D Outcomes No. 2016K000117, the National Research Foundation of Korea (NRF) grant funded by the Korean government (MSIP) No. 2011-0030079 and the Korean government (MEST) No. 2015R1D1A1A09057081. This work was also supported by a research grant from Kwangwoon University in 2016.

Appendix A. Supplementary material

Supplementary data associated with this article can be found in the online version at doi:10.1016/j.bios.2017.06.057.

References

Abdalla, S., Al-ameer, S.S., Al-Magaishi, S.H., 2010. Biomicrofluidics 4, 1–16.
Adhikari, K.K., Kim, N.Y., 2016. IEEE Trans. Microw. Theory Tech. 64, 319–327.
Aloraefy, M., Pfefer, T.J., Ramella-Roman, J.C., Sapsford, K.E., 2014. Sensors 14, 12127–12148.
Bahl, I., 2003. Lumped Elements for RF and Microwave Circuits. Artech House Inc., Norwood, MA, 301–306.
Balanis, C.A., 2005. Antenna Theory: Analysis Design third ed.. John Wiley & Sons, Inc., New York, 816–820.
Boukarkar, A., Lin, X.Q., Jiang, Y., Yu, Y.Q., 2017. IEEE Trans. Antennas Propag. 65, 850–854.
Dalmay, C., Pothier, A., Cheray, M., Lalloue, F., Jauberteau, M.O., Blondy, P., 2009. Int. J. Microw. Wirel. Technol. 1, 497–504.
Dhakal, R., Wang, C., Kim, E.S., Kim, N.Y., 2015. Appl. Phys. Lett. 106, 1–5.
Hu, R., Stevenson, A.C., Lowe, C.R., 2012. Biosens. Bioelectron. 35, 425–428.
ICH Harmonized Tripartite Guideline, 1996, Validation of analytical procedures: text and methodology Q2 (R1). In: Proceedings of the International Conference on Harmonization, pp. 11–12.
Kim, D.M., Kim, M.Y., Reddy, S.S., Cho, J., Cho, C.H., Jung, S.T., Shin, Y.B., 2013. Anal. Chem. 85, 11643–11649.
Kim, N.Y., Dhakal, R., Adhikari, K.K., Wang, C., Kim, E.S., 2015. Biosens. Bioelectron. 67, 687–693.
Lee, H.J., Lee, H.S., Yoo, K.H., Yook, J.G., 2010. J. Appl. Phys. 108, 1–6.
Lee, H.J., Lee, J.H., Moon, H.S., Jang, I.S., Choi, J.S., Yook, J.G., Jung, H., 2012. Sens. Actuators B 169, 26–31.
Lee, H.J., Lee, J.H., Choi, S., Jang, I.S., Choi, J.S., Jung, H., 2013. Appl. Phys. Lett. 103. http://dx.doi.org/10.1063/1.4816440.
Mirasoli, M., Bonvicini, F., Dolci, L.S., Zangheri, M., Gallinella, G., Roda, A., 2013. Anal. Bioanal. Chem. 405, 1139–1143.
Ouyang, H.M., Delouise, L.A., Miller, B.L., Fauchet, P.M., 2007. Anal. Chem. 79, 1502–1506.
Ricci, F., Moscone, D., Tuta, C.S., Palleschi, G., Amine, A., Poscia, A., Valgimigli, F., Messeri, D., 2005. Biosens. Bioelectron. 20, 1993–2000.
Rosa, S.L.L., Solheim, M., Diep, D.B., Nes, I.F., Brede, D.A., 2015. Sci. Rep., 1–11. http://dx.doi.org/10.1038/srep08339.
Siddiqui, S., Dai, Z.T., Stavis, C.J., Zeng, H.J., Moldovan, N., Hamers, R.J., Carlisle, J.A., Arumugam, P.U., 2012. Biosens. Bioelectron. 35, 284–290.
Tura, A., Sbrignadello, S., Cianciavicchia, D., Pacini, Giovanni, Ravazzani, Paolo, 2010. Sensors 10, 5346–5358.
Wang, J., 2001. Electroanalysis 13, 983–988.
Yilmaz, T., Foster, R., Wang, P., 2014. IEEE Trans. Microw. Theory Tech. 62, 3193–3204.
Yoon, G.W., 2011. Biosens. Bioelectron. 26, 2347–2353.
Suni, T., Henttinen, K., Suni, I., Makinen, J., 2002. J. Electrochem. Soc. 149, 348–351.
Zhang, X., Zhu, L., Liu, N.W., 2017. IEEE Trans. Antennas Propag. 65, 521–528.